

4624

## A Simple Method for Constrained Optimal Control RF Pulse Design

Sydney N. Williams<sup>1</sup>, Jon-Fredrik Nielsen<sup>2</sup>, Jeffrey A. Fessler<sup>3</sup>, and Douglas C. Noll<sup>2</sup>

<sup>1</sup>Imaging Centre of Excellence, University of Glasgow, Glasgow, United Kingdom, <sup>2</sup>Biomedical Engineering, University of Michigan, Ann Arbor, MI, United States, <sup>3</sup>Electrical Engineering and Computer Science, University of Michigan, Ann Arbor, MI, United States

### Synopsis

**Optimal control (OC) methods for RF pulse design are useful in cases where the small-tip angle (STA) approximation is violated. Furthermore, designs with physically meaningful constraints (e.g., RF peak amplitude and integrated power) eliminate the need for parameter tuning to create realizable pulses. In this abstract we introduce a constrained fast OC method that easily generalizes to a variety of RF pulse designs. We demonstrate with examples of SMS and spectral prewinding pulses in simulation and in vivo. The constrained fast OC method guarantees that RF pulses will meet physical constraints while outperforming their non-OC counterparts.**

### Introduction

RF pulse design is classically a regularized weighted least-squares optimization problem<sup>1</sup> under the small-tip angle (STA) approximation<sup>2</sup>. Recently, constrained pulse design<sup>3-5</sup> has become popular for designing physically realizable pulses without “check-and-redesign” parameter tuning.

Meanwhile, optimal control (OC) approaches have enabled the design of large-tip angle (LTA) pulses<sup>6-7</sup>. In this work we design constrained RF pulses via the fast OC method<sup>7</sup> that is simple and computationally inexpensive, but previous fast OC design methods did not include explicit constraints on RF amplitude and integrated power.

### Methods

The general pulse design problem we solve here is

$$\hat{\mathbf{b}} = \operatorname{argmin}_{\mathbf{b}} \|\operatorname{Bloch}(\mathbf{b}) - \mathbf{d}\|_{\mathbf{W}}^2$$

s. t. RF constraints

with RF pulse  $\mathbf{b}$ , target pattern  $\mathbf{d}$ , and weighting matrix  $\mathbf{W}$ . For LTA pulses, we linearize the Bloch equation with OC via perturbation updates<sup>7</sup> enforcing RF constraints directly at each update. This is unlike the STA approximation<sup>2</sup>, in which the Bloch equation evaluation of  $\mathbf{b}$  is substituted with the linear STA matrix  $\mathbf{A}$ . Figure 1 provides the pseudocode for this process. Importantly, the inner constrained problem is linear and can be solved with a variety of readily available methods (e.g., FISTA, CVX, etc.). The only values the user must provide the algorithm are the maximum number of iterations and % change in normalized root mean-squared error (NRMSE) for stopping criteria.

We designed two distinct RF pulse types to demonstrate the flexibility of this constrained fast OC approach. First, we designed a 90° simultaneous multislice (SMS) pulse with multiband factor MB=3 and compared to the standard implementation of phase shifted and summed slice-selective pulses, here Shinnar Le-Roux (SLR) pulses<sup>8</sup>. The SLR SMS pulse was designed with a time bandwidth product of 4, default SLR filter parameters, and a pulse length of 2.736 ms chosen to exactly meet peak RF amplitude constraints (0.2 G) after optimal phase modulation for peak amplitude reduction<sup>9</sup>. The constrained SMS MB=3 pulse was designed to have the same pulse length with constraints on peak amplitude and integrated RF power also matching the SLR SMS pulse.

Next, we designed a spectral prewinding slab-selective pulse pair<sup>10</sup> and obtained in vivo human brain results using the small-tip fast recovery (STFR) sequence<sup>11</sup> (FA/TE/TR=3.5°/3.82 ms/14.836 ms). Despite the small target flip angle, we previously found that prewinding pulses can exceed STA at intermediate pulse time points, making the OC approach useful. The STFR pulse pair was designed with a peak amplitude constraint of 0.2 G and the constrained OC pulses were compared to constrained pulses designed only using the STA approximation.

### Results

Figure 2 shows the RF and slice-select gradient waveforms for the SMS MB=3 pulses designed with the SLR method and the proposed constrained OC method. Figure 3 shows the simulated magnetization magnitude and slice profiles at TE for both pulses. Compared to a target magnetization of 90° MB=3 slices, the magnitude NRMSE is 0.10 for the SLR pulse pair and also 0.10 for the constrained pulse. The total compute time of the OC method was 5 minutes 22 seconds on an Intel Core i7-7700 CPU 3.60GHz processor.

Figure 4 shows the simulated slab profile and simulated magnetization (in two imaging planes) at TE for the slab-selective prewinding pulse designed with the constrained STA and fast OC methods. At TE the magnetization magnitude should be uniform and the phase should be zero. Compared to the target prewinding pattern, the simulated magnetization from the STA/OC pulses had magnitude NRMSEs of 0.29/0.19, phase RMSEs of 22.8°/11.4° and complex NRMSEs of 0.46/0.26, respectively. The total compute time of the OC method was 55 seconds compared to the STA approach's 24 seconds.

Figure 5 shows the experimental slab profiles and experimental images (in two imaging planes) for the slab-selective prewinding pulses. The slab profile is sharper and the phase image is flatter in the constrained method using the fast OC approach.

### Discussion and Conclusion

In our first example, a 90° MB=3 SMS pulse, the constrained fast OC pulse performs similarly to the comparative SMS pulse designed with the SLR algorithm. However the fast OC pulse took just around 5 minutes to design and directly met peak amplitude and integrated power constraints. Meanwhile, the SLR based pulse was designed heuristically by changing RF pulse lengths and slice select gradients until peak amplitude limits were met. In our second example, the fast OC method improved the performance (simulated NRMSE and in vivo image quality) for constrained slab-selective prewinding pulses in the STFR sequence. In both cases we showed that the fast OC approach can be applied efficiently to a variety of RF pulse designs and RF constraints.

### Acknowledgements

No acknowledgement found.

**References**

1. Yip, C. et al., Mag. Reson. Med., 54 (4), 2005.
2. Pauly, J. et al., J. Mag. Res., 81 (1), 1989.
3. Rund, A. et al., IEEE Trans. Med. Im., 37 (2), 2018.
4. Hoyos-Ildrobo, A. et al., IEEE Trans. Med. Im., 33 (3), 2014.
5. Guerin, B. et al., Mag. Reson. Med., 73 (5), 2015.
6. Conolly, S. et al., Mag. Reson. Med., 5 (2), 1986.
7. Grissom, W.A. et al., IEEE Trans. Med. Im., 28 (10), 2009.
8. Pauly, J. et al., IEEE Trans. Med. Im., 10 (1), 1991.
9. Wong, E., ISMRM, 2012.
10. Williams, S.N. et al., ISMRM, 2018.
11. Nielsen, J-F. et al., Mag. Reson. Med., 69 (3), 2013.

**Figures**

```

Algorithm 1 Pseudocode for designing constrained RF pulse with fast optimal control method?
Input: Target pattern  $\mathbf{d}$ , weighting matrix  $\mathbf{W}$ , excitation trajectory  $\mathbf{k}$ , and RF hardware constraints
Output: RF pulse  $\mathbf{b}$ 
Initialization:
1. Using  $\mathbf{k}$ , construct STA approximation matrix  $\mathbf{A}$ 
2. Design  $\mathbf{b}^1$  by solving STA problem with RF constraints (Eq. (1))
3. Use  $\mathbf{b}^1$  with Bloch simulator to compute  $\mathbf{M}^1$  and construct optimal control perturbation matrix  $\tilde{\mathbf{A}}_{OC}^1$  from  $\mathbf{b}^1$  and  $\mathbf{M}^1$ 
4.  $\text{NRMSE}^0 = 1$ ,  $\text{NRMSE}^1 = \text{NRMSE}(\mathbf{b}^1)$ ,  $p = 1$ 
Optimal Control Perturbation Update:
5. while ( $p = \text{max no. iter}$  and  $\text{NRMSE}^p <= 0.9999 + \text{NRMSE}^{p-1}$ ) do
6.   Update target perturbation  $\tilde{\mathbf{M}}^{p+1} = \mathbf{M}^p - \mathbf{M}^p$ 
7.   Design constrained perturbation RF pulse to match target perturbation (adapting STA problem)

$$\tilde{\mathbf{b}}^p = \underset{\tilde{\mathbf{b}}}{\text{argmin}} \|\tilde{\mathbf{A}}_{OC}^p \tilde{\mathbf{b}} - \tilde{\mathbf{M}}^{p+1}\|_2$$

   s.t. constraints on  $\tilde{\mathbf{b}} + \mathbf{b}^p$ 
8. while ( $j < \text{max no. iter}$ ) do
9.   Add perturbation RF pulse to previous designs,  $\mathbf{b}^{p+1} = \tilde{\mathbf{b}}^j + \mathbf{b}^p$ 
10.  Simulate  $\mathbf{M}^{p+1}$ , compute  $\text{NRMSE}^{p+1}$ , construct OC matrix  $\tilde{\mathbf{A}}_{OC}^{p+1}$ 
11.  if ( $\text{NRMSE}^{p+1} > 0.9999 + \text{NRMSE}^p$ ) then
12.     $\tilde{\mathbf{b}}^j = \tilde{\mathbf{b}}^j$ 
13.     $j = j + 1$ 
14.  else
15.     $j = \text{max no. iter.}$ 
16.  end if
17. end while
18.  $p = p + 1$ 
19. end while
20. return  $\mathbf{b}^p \in \mathcal{C}^N$ 
    
```

**Figure 1.** Algorithm for constrained RF pulse design using the fast optimal control method. Previous fast optimal control methods (Grissom, IEEE TMI 2009) did not impose direct RF constraints. In this fast OC method, perturbation updates are simulated for designed pulses that are added to the current RF pulse at each iteration, stopping when the RF pulse is no longer improving (in the NRMSE sense) or a maximum number of iterations is reached.

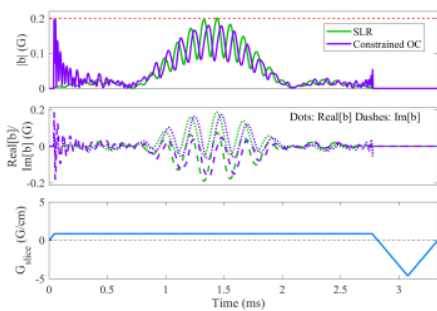


**Figure 2.** Top row: RF magnitude waveforms for the SLR (green) and constrained OC (purple) slice-selective MB=3 90° pulse. Middle row: real (dots) and imaginary (dashes) RF waveforms for the SLR SMS (green) and constrained OC SMS (purple) pulse. Bottom row: Slice-select gradient (4mm slice) and associated rephaser gradient.

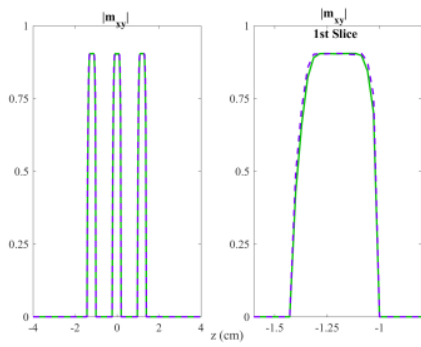


**Figure 3.** Left: Simulated slice profiles at TE for SLR (green dots) and constrained OC (purple dashes) SMS MB=3 pulses. Right: Zoomed in profile of 1st slice for SLR and constrained OC SMS MB=3 pulses. In general, the simulated magnetization magnitude are nearly identical.

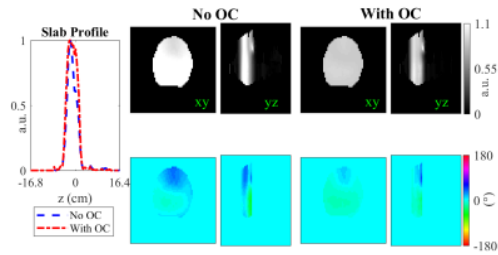


**Figure 4.** Constrained, slab-selective spectral prewinding pulses simulated at TE. Top row: magnetization magnitude for STA (no OC, center), and OC pulse (right). Bottom row: magnetization phase for STA (no OC, center), and OC pulse (right). Left: mean slab profile in x dimension for both pulses.

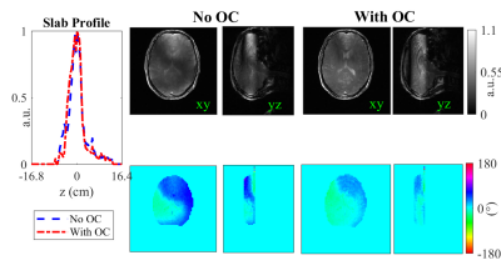


**Figure 5.** Experimental STFR images from the constrained, slab-selective spectral prewinding pulses simulated in Figure 4. Top row: magnetization magnitude for STA (no OC, center), and OC pulse (right). Bottom row: magnetization phase for STA (no OC, center), and OC pulse (right). Left: mean slab profile in x dimension for both pulses.